Fuel 202 (2017) 631–640

Contents lists available at ScienceDirect

Fuel

journal homepage: www.elsevier.com/locate/fuel

Full Length Article

Prediction of thermal behavior of trickle bed reactors: The effect of the pellet shape and size

María J. Taulamet, Néstor J. Mariani, Guillermo F. Barreto, Osvaldo M. Martínez *

PROIRQ, Departamento de Ingeniería Química, Facultad de Ingeniería, UNLP, La Plata, Argentina
Centro de Investigación y Desarrollo en Ciencias Aplicadas "Dr. J.J. Ronco" (CINDECA) CCT La Plata – CONICET – UNLP, calle 47 No. 257, CP B1900AJK La Plata, Argentina

ARTICLE INFO

Article history:
Received 15 May 2016
Received in revised form 31 March 2017
Accepted 6 April 2017
Available online 24 April 2017

Keywords:
Trickle-bed reactors
Heat transfer
Two dimensional pseudohomogeneous model
Effective radial thermal conductivity
Wall heat transfer coefficient

ABSTRACT

Heat transfer plays an important role in several applications of packed bed reactors with cocurrent downflow of liquid and gas (widely known as trickle-bed reactor – TBR).

A literature survey shows that the amount of articles dealing with the prediction of heat transfer rates between a TBR and an external heating or cooling source is limited for spherical catalyst pellets and definitively scarce for other pellet shapes as cylinders and multilobes.

Results from an experimental program devoted to study heat transfer between a TBR and an external jacket, employing spherical and cylindrical particles and a commercial trilobe pellet, are presented. A wide range of gas (air) and liquid (water) flow rates were covered corresponding to low and high interaction regime. A two dimensional pseudohomogeneous model was employed to represent the thermal behavior of the packed bed. Values of the effective radial thermal conductivity and the wall heat transfer coefficient were obtained by regression of radial temperature profiles for three different bed lengths. Finally, expressions to estimate both parameters for the different particle shapes were developed, thus providing a useful predictive tool, not available in the literature up to the best of our knowledge.

1. Problem statement

Trickle–bed reactors (TBRs) are widely employed in a variety of processes from traditional fields as chemical, petrochemical and petroleum industries to relatively novel applications in biochemical, electrochemical and waste water treatments [1].

The complex fluid-dynamic behavior of TBR introduces several uncertainties in the estimation of transport parameters usually employed in the reactor modeling. Among the parameters needed to perform catalytic reactor simulations are particularly important those associated to heat transfer processes.

Different catalytic processes at industrial scale carried out in TBRs, such as the production of methyl isobutyl ketone or the conversion of natural gas to liquid hydrocarbons (GTL) [2–4], require exchanging heat with an auxiliary fluid. In these cases, the heat transfer process determines the reactor behavior. In addition, an adequate prediction of heat transfer rates is needed when using laboratory and bench scale TBRs to analyze the behavior of a given catalyst due to the usual requirement to operate isothermally aiming at facilitating the analysis of the experimental results [5]. It is also worth mentioning that non-stable *hot spots* can certainly arise both in industrial reactors [6] and laboratory reactors under fully controlled conditions [7].

In a recent article Taulamet et al. [8] have reviewed literature information about heat transfer in TBRs. The authors found that few experimental studies deal with particle shapes different from spherical, in spite of the fact that, for example, multilobe pellets are extensively employed in industrial TBRs [9,10]. Also, in the above mentioned review it is concluded that the two-dimensional pseudohomogeneous model is a suitable alternative to represent the reactor behavior if a detailed simulation is intended.

In a previous study [11] results from heat transfer experiments using spheres of different sizes were reported. The purposes of this contribution are to present new experimental data for cylinders and trilobe pellets, compare them with those for the spheres and reach suitable expressions to estimate the two parameters of the two-dimensional pseudohomogeneous model (*i.e.*, effective radial thermal conductivity and wall heat transfer coefficient) for the whole set of particles shape and sizes.

* Corresponding author at: PROIRQ, Departamento de Ingeniería Química, Facultad de Ingeniería, UNLP, La Plata, Argentina.
E-mail address: ommartin@ing.unlp.edu.ar (O.M. Martínez).

http://dx.doi.org/10.1016/j.fuel.2017.04.031
0016-2361/

Nomenclature

a	bed to particle diameter ratio, d_t/d_{eq} [–]
A_t	bed cross-section area, [m^2]
Bi	Biot number, $(h_w R_t)/k_{er}$ [–]
b_n	nth eigenvalue of the Eq. (6e), [–]
C_P	specific heat, [$J\,kg^{-1}\,K^{-1}$]
d_P	particle diameter, [m]
d_{eq}	equivalent diameter, [m]
d_t	bed tube diameter, [m]
G	gas superficial mass velocity, [$kg\,m^{-2}\,s^{-1}$]
H	particle length, [m]
h_C	jacket heat transfer coefficient, [$W\,m^{-2}\,K^{-1}$]
h_T	bed to tube wall overall heat transfer coefficient, [$W\,m^{-2}\,K^{-1}$]
h_w	wall heat transfer coefficient, [$W\,m^{-2}\,K^{-1}$]
J_0, J_1	Bessel function of first kind, order zero and one, respectively, [–]
k	fluid thermal conductivity, [$W\,m^{-1}\,K^{-1}$]
k_{er}	effective radial thermal conductivity, [$W\,m^{-1}\,K^{-1}$]
L	liquid superficial mass velocity, [$kg\,m^{-2}\,s^{-1}$]
Nu_w	Nusselt number, $h_w\,d_{eq}/k_L$, [–]
Pr	Prandtl number, $C_P\,\mu\,/k$, [–]
r	radial coordinate, [m]
Re	Reynolds number, $G\,d_{eq}/\mu_G$ or $L\,d_{eq}/\mu_L$ [–]
R_t	bed tube radius, [m]
S_p	external surface area of the particle, [m^2]
T	temperature, [K]
u	superficial velocity, G/ρ_G or L/ρ_L, [ms^{-1}]
V_P	particle volume, [m^3]

Symbols

β_T	total liquid saturation based on overall bed void fraction (ratio between the total liquid volume and the overall bed void volume), [–]
ε	overall bed void fraction, [–]
ϕ	particle aspect ratio, d_p/H, [–]
ρ	density, [$kg\,m^{-3}$]
μ	dynamic viscosity, [Pa s]
ν	parameter in the Eq. (13b)
ω	parameter in the Eq. (13b)

Subscripts and subscripts

C	heating fluid
E	bed exit
G	gas
0	bed inlet
L	liquid
r	radial
w	wall
F	global

2. Experimental set-up

Beds of spheres and cylinders of different sizes and a commercial trilobe catalyst (a spent catalyst employed in a hydrotreating process) have been studied. The results for spheres include those previously obtained by Mariani et al. [11]. The trilobe catalyst presents a normal Gaussian distribution of lengths (H) in the range 2.8–13.9 mm with a mean value of 6.6 mm, while the sizes of spheres and cylinders are practically uniform (see Table 1).

No universally accepted criterion was found in the literature about the characteristic size to be used for heat transfer analysis in the case of non-spherical pellets. The equivalent diameter (d_{eq}) here employed is the one of a sphere that has the same ratio between the actual volume and the actual external surface area of the particle, the so-called Sauter diameter [12]. The pellet shape for cylinders and trilobe particles was characterized, as heat transfer process concerns, by the ratio between diameter and length, $\phi = d_p/H$. It is important to clarify that in the case of the trilobe pellet, d_{eq} was calculated on the basis of the actual external surface area, while ϕ was evaluated by considering the diameter d_p of the lobe envelope.

Particle sizes, bed to particle diameter ratios ($a = d_t/d_{eq}$), particle aspect ratios (ϕ) and overall bed void fractions (ε) are reported in Table 1.

Water and air under ambient conditions of pressure and temperature were fed cocurrently downwards. The superficial mass velocities of the water (L) and air (G) were varied between 2.4 and 13.9 $kg\,m^{-2}\,s^{-1}$ and between 4.5 10^{-2} and 0.83 $kg\,m^{-2}\,s^{-1}$, respectively, thus covering conditions corresponding to the so-called high and low interaction regimes [13–15]. The whole set of experimental conditions (gas and liquid superficial mass velocities and particle shapes) are reported in Table 2.

A scheme of the experimental set-up is shown in Fig. 1. It consists of a tube of 51.4 mm in diameter, surrounded by a jacket divided into three sections, identified as lower, middle and upper sections. Hot water fed at 80 °C can pass either through the lower section, through the lower and middle sections or through the three sections of the jacket altogether, thus allowing three different bed lengths (27, 47 and 87 cm) for heat transfer. The heating water flow rate was high enough to maintain nearly isothermal conditions within the jacket.

Temperature was measured at the inlet and outlet of each section of the jacket; on the bed axis (r = 0) at the height z = 0 where the active heat transfer section begins, $T_0(0)$; at the outlet of the liquid stream; at nine points distributed radially and angularly inside the bed over the cross section at about 30 mm above the supporting plate as depicted in Fig. 2, and at three axial positions

Table 1
Information of particles used in the experiments.

Authors	Shape	Material	Dimensions (mm)	d_{eq}[2](mm)	$\phi = d_p/H$	$a = d_t/d_{eq}$	ε
Mariani et al. (2001)	Sphere 1	Glass	d_p = 1.5	1.5	1	34.27	0.39
	Sphere 2	Glass	d_p = 3.0	3.0	1	17.13	0.40
This contribution	Cylinder 1	Glass	d_p = 2 H = 6.5	2.6	0.308	19.77	0.38
	Cylinder 2	Glass	d_p = 8.74 H = 11.8	9.6	0.741	5.35	0.37
	Trilobe	Porous α-Alumina	d_p[1] = 2.6 H = 6.6	2.12	0.394	24.19	0.37

[1] d_p for the trilobe particle is defined as the diameter of the envelope of the lobes.
[2] d_{eq} = equivalent (Sauter) diameter: diameter of a sphere with the same ratio of the actual volume to the actual external surface area of the particle.

Table 2
Summary of the experimental operating conditions.

Shape	L [kg m^{-2} s^{-1}]	G .10^2 [kg m^{-2} s^{-1}]
Cylinder 1	2.4/3.2/4.5/6.0/8.0/9.6/12.0/13.9	14
	4.5/10.0	41
	9.6	55
	4.5	83
Cylinder 2	3.6/4.5/6.0/8.0/10.0/12.0	4.5
	3.2/4.5/6.0/8.0/10.0/11.6	14
	4.5	54
Trilobe	2.4/4.4/8.0/13.9	4.5
	2.4/4.5/8.0	14
	2.4	53

within the tube-wall. All the temperature readings were recorded by a data acquisition system.

The top of the tube (indicated in Fig. 1 as calming section) was packed with particles of the same size and shape as those used in the jacked sections of the bed (*i.e.*, those active for heat transfer). The calming section was included to enable gas-liquid thermal equilibrium and to provide a uniform liquid distribution at the inlet of the jacked sections.

For each experimental condition, defined by a given packing size and shape, water and air flow rates, between 4 and 8 replicates were performed for each heat transfer length. Before performing each replicate, the bed was fluidized by water to provide different random packings. The whole procedure for each replicate demanded about 3–4 h. After reaching steady state conditions, the recorded temperature sets (about 2000) were averaged to obtain the values used for analytical purposes.

Some other details concerning the experimental set-up and operating procedure can be found in Mariani [16] and Taulamet [17].

3. Model formulation

Aiming to analyze the experimental heat transfer data the two-dimensional pseudo-homogeneous plug flow model (2DPPFM) was adopted.

The energy balance considering steady state operation, no temperature difference between phases, negligible axial thermal conduction and plug flow, reads [8]:

$$\left(LC_{pL} + GC^*_{pG}\right)\left[\frac{\partial T}{\partial z}\right] = \frac{1}{r}\frac{\partial}{\partial r}\left[k_{er} r \frac{\partial T}{\partial r}\right] \tag{1a}$$

C_{pL} is the liquid specific heat and C^*_{pG} a modified heat capacity that accounts for the calculated as:

$$C^*_{pG} = \frac{\hat{H}_E - \hat{H}_0}{\bar{T}_E - \bar{T}_0} \tag{1b}$$

$\hat{H}_0$ and $\hat{H}_E$ are the enthalpies of saturated air-steam per unit mass of dry air at the bed-inlet average temperature $(\bar{T}_0)$ and at the bed-exit average temperature $(\bar{T}_E)$, respectively.

To solve Eq. (1a) one inlet and two boundary conditions are needed.

Assuming radial symmetry the boundary condition at the bed axis is:

$$\partial T/\partial r = 0 \text{ at } r = 0 \tag{2}$$

Considering a uniform value of effective radial thermal conductivity (k_{er}), the most frequently employed second boundary condition establishes a thermal resistance ($1/h_w$) just concentrated at the tube wall. According to the experimental set-up facilities, axial temperature profile along the tube wall cannot be adequately measured so as to check its uniformity. Nonetheless, it was possible to verify that the heating water temperature (T_C) remains virtually constant inside the jacket, due to the high water flow rate [16]. Thus, introducing a heat transfer coefficient at the jacket side (h_C), the second boundary condition can be set as:

$$k_{er}\frac{\partial T}{\partial r} = h^F[T_C - T(r = R_t)] \text{ at } r = R_t \tag{3}$$

where T_C is assumed to be constant and h^F is defined as:

$$\frac{1}{h^F} = \frac{1}{h_w} + \frac{1}{h_C} \tag{4}$$

It is important to mention that h_C was independently measured by Mariani [16] for a given set of conditions in the same experimental set-up and values of $1/h_w$ were typically ten times larger than $1/h_C$. Thus, as $1/h_w$ is the controlling resistance to heat transfer h_w can be properly determined.

At the inlet of the active heat transfer section (z = 0), a radial temperature profile is considered:

$$T = T_0(r) \text{ at } z = 0 \tag{5}$$

The solution of Eq. (1a), with boundary conditions (2) and (3) and inlet condition (5), leads to

$$\frac{T_C - T(r,z)}{T_C - T_0(0)} = 2\sum_{n=1}^{\infty} C_n \frac{J_0(b_n r/R_t)\left[\exp\left(-b_n^2 z^*\right)\right]}{\left[1 + \left(b_n/Bi^F\right)^2\right] J_1^2(b_n)} \tag{6a}$$

where:

$$C_n = \frac{1}{R_t^2}\int_0^{R_t}\left[\frac{T_C - T_0(r)}{T_C - T_0(0)}\right] J_0(b_n r/R_t) r dr \tag{6b}$$

$$z^* = \frac{\pi k_{er}}{\left(LC_{pL} + GC^*_{pG}\right)A_t} z \tag{6c}$$

$$Bi^F = \left(h^F R_t\right)/k_{er} \tag{6d}$$

b_n are the positive roots of the following equation

$$Bi^F J_0(b_n) = b_n J_1(b_n) \tag{6e}$$

To avoid a strong disturbance of the packing with the insertion of a set of temperature probes at the inlet of the heat transfer region, only the value $T_0(0)$ at the axis was measured. As the whole profile $T_0(r)$ is not known, a possible approach would be regarding the coefficients C_n as additional fitting parameters in the regression procedure. However, Mariani [16] discussed that this approach turns out to be impractical if the number of the needed terms in Eq. (6a) is large (say, more than 3–4). Simultaneously, it was checked that for typical shapes of $T_0(r)$, the terms in the series of Eq. (6a) for n > 1 are considerably smaller than the first one at values of z^* where the radial temperature profiles are measured [16]. Therefore, only the first coefficient C_1 was employed as a fitting parameter, while the remaining ones were assumed to be related to C_1 as for uniform inlet temperature [8]:

$$C_n = C_1\frac{J_1(b_n)}{J_1(b_1)}\frac{b_1}{b_n} \tag{7}$$

Summing up, the fitting parameters are C_1, k_{er} and h^F.

Aiming to perform the regression analysis, radial temperature profiles for different bed lengths are employed as input data and a parameter estimation routine using the non-linear least square method with the following objective function is used:

$$S(C_1, k_{er}, h^F) = \sum_{i=1}^{N_{obs}}\left[T^{exp}(r_i, z_i) - T^{pred}\left(r_i, z_i, C_1, k_{er}, h^F\right)\right]^2 \tag{8}$$

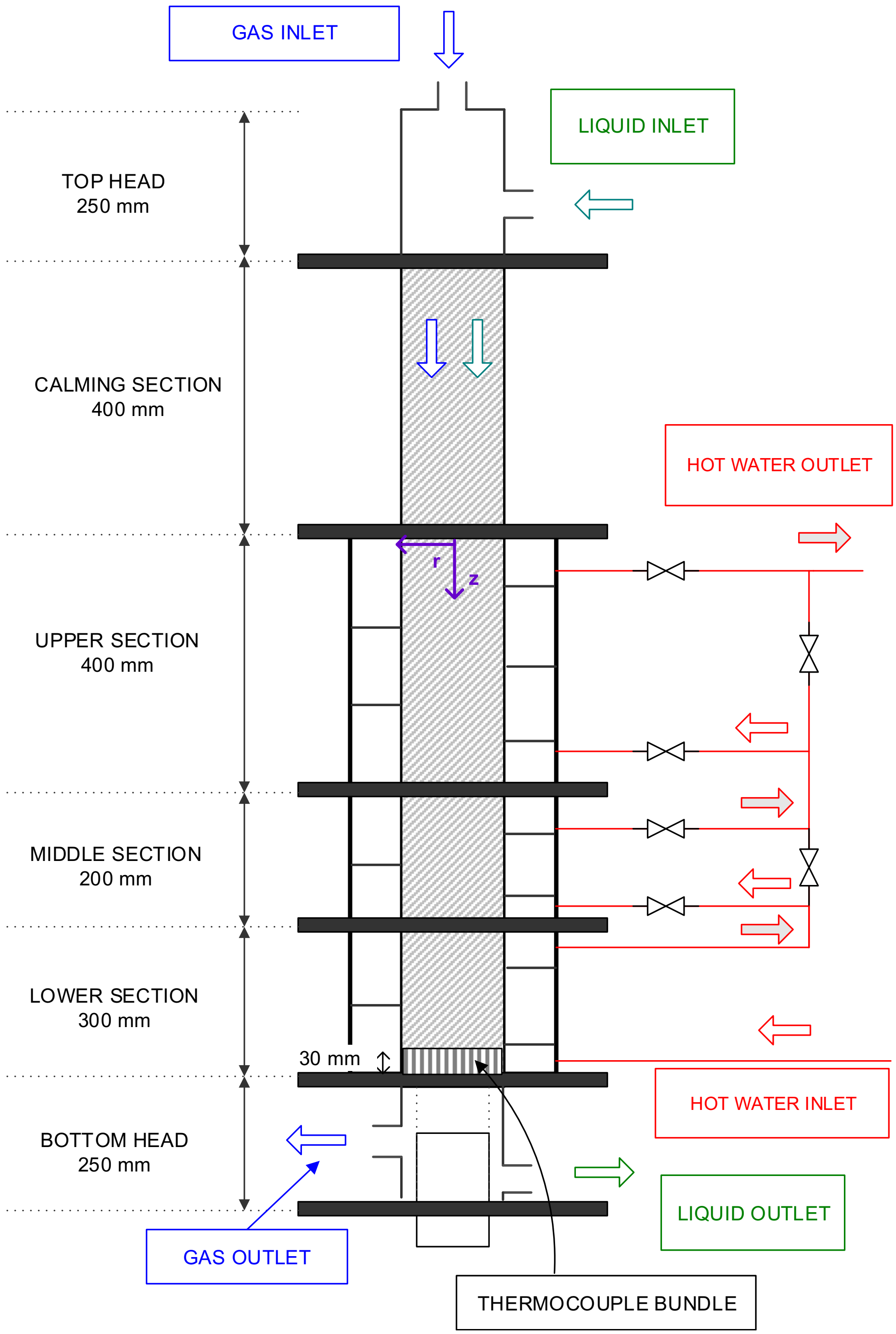

Fig. 1. Sketch of the experimental set-up.

where $T^{exp}(r_i, z_i)$ are experimental temperature data, $T^{pred}\left(r_i, z_i, C_1, k_{er}, h^F\right)$ are the values predicted by the model (Eqs. (6a)–(6e)) and N_{obs} is the number observed temperatures for each experimental condition defined by given packing size and shape and water and air flow rates.

It is important to mention that no convergence problems were detected in the regression procedure. In addition, the confidence intervals for all the values of Nu_w and k_{er}, expressed as $\Delta k_{er}/k_{er}$ and $\Delta Nu_w/Nu_w$, were always less than 13.3% and 15.9% for the trilobe pellets, less than 16.1% and 15% for cylinders 1 and less than 38.8% and 12.1% for cylinders 2, respectively.

It is worth recalling that radial temperature profiles were measured for three different bed lengths 27, 47 and 87 cm, respectively. Some of the data for the longest active bed and low superficial liquid mass velocities were not employed in the regression because the radial temperature profiles were almost uniform and close to the heating water temperature T_C [17]. The

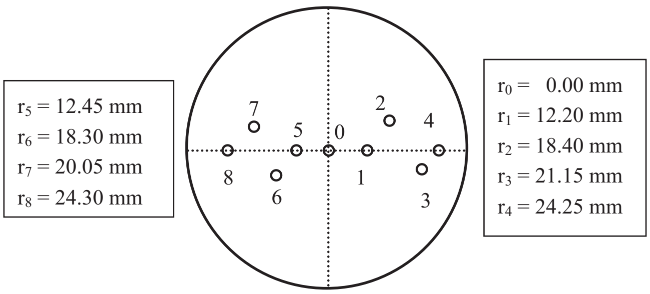

Fig. 2. Sketch of the supporting plate of the bed including the position of the nine thermocouples.

thermo-physical properties of the fluids were evaluated at 40 °C, being this value fully representative of the inlet and exit average temperature for the whole set of experiments.

4. Results and discussion

4.1. Experimental results and correlation for the wall heat transfer coefficient (h_w)

Mariani et al. [18] discussed the effect of the bed to particle diameter ratio (a) on the heat transfer parameters h_w and k_{er} for spherical particles. It was shown that the 2DPPFM cannot be suitably applied when the bed to particle diameter ratio (a) is smaller than around 15. The main reason found for this observation was a considerable higher liquid velocity close to the wall than in the bed core. This feature presents little effect for large values of a, but it was most significant at the lower values of a. A two-region model was successfully employed by Mariani et al. [18] to cope with the behavior of spherical particles at low bed to particle diameter ratios. Furthermore, it was proved that the behavior of such a model nearly coincide with that of the 2DPPFM at larger values of a. In particular, Mariani et al. [18] showed that values of the wall heat transfer coefficient h_w resulting from the use of the 2DPPFM were abnormally high for spheres with $a < 15$. The present experiments include cylinders 2 in Table 1 that render $a = 5.35$. Therefore, it is relevant to disclose if cylinders 2 show a similar behavior as that of spheres at low a. The results of h_w (expressed as Nu_w) are plotted in Fig. 3 against liquid Reynolds number (Re_L) for the set of packings in Table 1 (the equivalent diameter d_{eq} is used in the definition of Nu_w and Re_L). Values of a for the cylinders 1 and trilobe pellets are higher than 15 (see Table 1) and it can be observed in Fig. 3 that their values of Nu_w are similar. Instead, values of Nu_w for cylinders 2 are much larger than for cylinders 1 and trilobe pellets. Eq. (10), discussed further ahead in this section, is proposed to correlate Nu_w for the set of packings in Table 1, but excluding cylinders 2. When this expression is employed for cylinders 2, the dotted curve in Fig. 3 arises. The difference between this curve and the experimental data reinforce the fact that the low value $a = 5.35$ introduces a distinct effect that the 2DPPFM is not able to quantify.

Therefore, the results obtained with cylinders 2 have not been considered in this contribution to develop correlations for h_w and k_{er}. They can be re-analyzed using a two-region model, as the one proposed by Mariani et al. [18].

It has been previously shown by Mariani et al. [11] that the gas superficial mass velocity G has a little impact on heat transfer parameters for spheres. Then, the results for each spherical size have been grouped irrespective of the value of G. On the contrary, Nu_w values for cylinder 1 ($d_{eq} = 2.6$ mm) and trilobe pellets have been grouped in Fig. 3 according to those presenting low or high gas Reynolds number (Re_G). It is evident that, in spite of the signif-

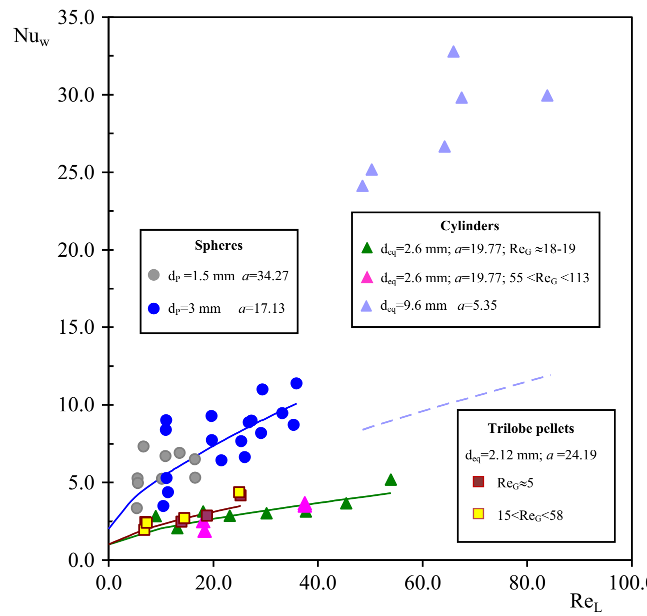

Fig. 3. Nu_w vs. Re_L for the particles in Table 1. Symbols: experimental data. The curves are predictions from Eq. (10) for each type of packing. The dotted-curve corresponds to the large cylinders ($d_{eq} = 9.6$ mm).

icant change in Re_G (around 12 times for trilobe pellets and 6 times for cylinders 1), Nu_w does not show any noticeable variation. Therefore, within the studied range of gas superficial mass velocities, G does not seem to exert any appreciable influence on h_w, irrespective of particle shape.

In a previous contribution Taulamet et al. [19] showed that it is feasible to treat together results from heat transfer experiments in TBRs corresponding to the low (gas continuous) and high interaction regimes, provided that the interaction between both fluid phases is not intense. Therefore, the results displayed in Fig. 3 were used for developing a predictive expression, include data obtained in the low and high interaction regimes, but those corresponding to very large values of L and/or G were disregarded.

As a starting point to get a suitable general correlation for Nu_w, the expression proposed by Mariani et al. [11] for spheres has been chosen. From Fig. 3, it can be visualized a significant effect of L (Re_L), which is similar in nature (*i.e.*, Nu_w monotonically increases with Re_L) for spheres, cylinders 1 and trilobe pellets. Thus, resorting to the usual assumption that conductive and convective contributions are additive, the following type of expression is proposed,

$$Nu_w = Nu_{w0} + a_w Re_L^{b_w} Pr_L^{1/3} \tag{9}$$

where Nu_{w0} is the conductive contribution to heat transfer at the wall, which corresponds to the stagnant contribution, and a_w and b_w are fitting parameters. Fitting values of Nu_{w0}, a_w and b_w have been first obtained for each type of packing by minimizing the sum of squared differences between predicted $\left(Nu_w^{pred}\right)$ and experimental $\left(Nu_w^{exp}\right)$ values. Values thus obtained for b_w did not differ significantly for the different particles. On the contrary, considerable differences in the values of a_w and Nu_{w0} arose. The fitting values of Nu_{w0} could be grouped in two sets: spheres and cylindrical particles (cylinders 1 and trilobe pellets). On the other hand, it was found that effect of particle shape on a_w could be captured by expressing: $a_w = \alpha\, \phi^{\gamma}$, where α and γ are fitting constants independent of particle shape. On this basis, a final regression analysis on N = 46 experimental data led to the following expression:

$$Nu_w = Nu_{w0} + 0.4\phi\, Re_L^{0.7} Pr_L^{1/3} \tag{10}$$

where

$$\mathrm{Nu_{w0}} = \begin{cases} 2 & \text{(spheres)} \\ 1 & \text{(cylindrical particles)} \end{cases} \tag{11}$$

The average absolute deviation defined as,

$$\varepsilon_{\mathrm{Nu_w}} = \frac{100}{N}\sum_{i=1}^{N}\frac{\left|\mathrm{Nu_{w,i}^{pred}} - \mathrm{Nu_{w,i}^{exp}}\right|}{\mathrm{Nu_{w,i}^{exp}}}$$

was 15.2% with an even distribution of 23 positive and 23 negative deviations. Concerning the results for spheres, $\varepsilon_{\mathrm{Nuw}}$ = 18%, while for cylinders 1 and trilobe particles $\varepsilon_{\mathrm{Nuw}}$ = 11%.

Eq. (10) is valid under the following conditions (employing water and air as fluids):

$1.5 \le d_{eq}\ [\mathrm{mm}] \le 3$; $17.1 \le a \le 34.3$; $5.4 \le Re_L \le 53.9$
$0.0029 \le u_L\ [\mathrm{m/s}] \le 0.014$; $0.31 \le \phi \le 1$; $2 \le Re_G \le 113$
$0.023 \le u_G\ [\mathrm{m/s}] \le 0.74$

Values of $\mathrm{Nu_{w0}}$ are expected to depend on the thermal conductivity of the liquid and of the packing material. Therefore, the values reported in Eq. (11) can be confidently used if the thermal conductivity of the fluid and the particles does not depart much from that of water and for ceramic materials.

A satisfactory agreement between the experimental data and values from Eq. (10) can be appreciated in Fig. 3, in particular, for the cylindrical particles (cylinders 1 and trilobe pellets). The general trend for spherical particles is also satisfactorily predicted, in spite of the scatter of the experimental data. The noticeable difference in the scattering for spheres as compared with cylindrical particles may be assigned to the low contribution of wall heat transfer resistance ($R_w = 1/h_w$) to the overall bed thermal resistance for spheres (see Section 4.3), which makes the experimental determination of h_w more inaccurate.

It is also observed from Fig. 3 that the $\mathrm{Nu_w}$ values for cylinders 1 and trilobe pellets are, on average, 2 and 3 times lower than for spheres. The reasons for such differences can be found in the different fluid-dynamic behavior of cylindrical particles and spheres in the near wall region. In this sense, it is worth to mention that Giese et al. [20] performed experimental measurements of the radial velocity profile for water flowing (single phase flow) in a tube packed with cylinders and spheres of different sizes. The authors found that the superficial-velocity radial profile is nearly uniform for cylinders, but local velocities are neatly higher for spheres up to distances of around $d_p/2$ from the wall. These results suggest that the fraction of liquid that circulates in the near wall region suffers, on average, larger friction forces for a cylindrical packing than for the spherical one. Of course fluid-dynamics for trickling flow is different than for a single-phase flow (as TBR is gravity-driven flow while single-flow is forced convection and also the total liquid saturation is always less than the overall bed void fraction in TRB), but a correlation most probably holds. As h_w will strongly depend on the local superficial velocity close to the wall, values for spheres will be consequently higher than for cylinders, when compared at the same average superficial velocity (*i.e.*, at the same value of Re_L).

4.2. Experimental results and correlation for the effective radial thermal conductivity (k_{er})

Aiming to develop a correlation for k_{er}, the experimental data collected for the packing in Table 1, but excluding cylinders 2 for the reasons mentioned in Section 4.1, and a literature database [8] were employed. The purpose of incorporating the literature data was to broaden the set of operating and geometric conditions (*i.e.*, bed to particle diameter ratios, gas and liquid superficial mass velocities) and to include different experimental set-ups and procedures for data reduction.

Concerning the flow regime, data of low interaction regime and data of high interaction regime not far from the transition have been included, as in the case of h_w (Section 4.1).

In a recent review Taulamet et al. [8] showed that the correlations from Lamine et al. [21] and Mariani et al. [11] present the lowest errors in the predictions of k_{er} in low interaction regime when such expressions are compared against experimental data.

In regards to the effect of the liquid superficial flow velocities, both correlations predicts $k_{er} \propto L^b$, with b < 1; this aspect differs from single-phase flow expressions that set a linear relationship, b = 1. This value is supported by the fluid lateralization model originally derived by Ranz [22], which predicts the linear relationship as a consequence of the proportional increase in the interstitial velocity as L increases. In the case of two-phase flow an increase in L also causes an increase in the total liquid saturation (β_T), and the net effect of L on the interstitial velocity is therefore somewhat less than for the single-phase flow.

The effect of G on k_{er} is much weaker that the effect of L, most probably on account of the fact that usual values of G are definitely much lower than L. The effect exerted by G on k_{er} can be adequately introduced through β_T, as proposed by Lamine et al. [21] and Mariani et al. [11] in their correlations.

Recognizing the fact that in this study the liquid phase is always water it is stated that $k_{er} \propto Pr$, as Lamine et al. [21] and Mariani et al. [11] suggested. From the above discussion the following expression is proposed to correlate the k_{er} data

$$k_{er} = k_{e0} + a_k Re_L^{b_k} \beta_T^{c_k} Pr_L k_L \tag{12}$$

k_{e0}, a_k, b_k and c_k are fitting parameters depending, in principle, on particle shape.

To estimate the total liquid saturation, Larachi et al. [23] expression will be employed.

A preliminary analysis [8] indicated that the conductive term k_{e0} represents a very small contribution for the range of experimental liquid flow rates. Consequently, k_{e0} cannot be correctly discriminated for different particle shapes, and therefore a common value was included as a fitting parameter.

Fitting of the experimental data just for spheres leads to $c_k \approx -1$ and $b_k \approx 1$. These values are also assumed to be valid for all shapes. Then, Eq. (12) is reduced to

$$k_{er} = k_{e0} + a_k \frac{d_{eq} L C_{pL}}{\beta_T} \tag{13a}$$

From a physical point of view, expression (13a) state that k_{er} linearly depends on the liquid interstitial velocity [*i.e.*, $u_{Li} = L\,\rho_L/(\varepsilon\,\beta_T)$]. On the other hand, as discussed before, the effect of G on k_{er} can be adequately considered by its influence on β_T. In the single-phase flow literature, the parameter a_k is employed to introduce the effect of the bed to particle diameter ratio (a), reaching an asymptotic value for $a \to \infty$. Here, a_k has been also assumed to depend on particle shape through the ratio ϕ. Thus, expression (13b) is considered for a_k.

$$a_k = \omega \frac{\phi^m}{1 + \zeta a^{\nu}/\phi^n} \tag{13b}$$

The data for spherical packing reveal that ν = 2 can be satisfactorily used in Eq. (13b), just as suggested by Fahien and Smith [24]. This value was adopted for all particle shapes. In this way, there remain 5 fitting parameters in Eq. (13): k_{e0}, ω, ζ, m and n. The optimum values for them have been obtained by minimizing the sum of squared differences between 171 experimental values of k_{er} and their predictions from the proposed model. The final correlation becomes

$$k_{er} = 0.87k_L + 1/9\frac{\phi^{-0.4}}{(1+100a^2/\phi^{1.8})}\frac{d_{eq}LC_{pL}}{\beta_T} \quad (14)$$

The average relative deviation of Eq. (14) was 15.7%, with a reasonably balanced error distribution (71 positive and 100 negative values). Spherical packing showed an average deviation of around 17%, while that for non-spherical particles was 11%.

The value $\omega = 1/9$ arising when $a \to \infty$ for spheres ($\phi = 1$) lies in the typical range reported for single-phase flow in packed bed. In his review article, Dixon [25] reported values of ω from 1/12 to 1/8.

Fig. 4 shows a parity plot for k_{er}, which includes the whole set of experimental data employed in the regression (the sources of experimental data are also identified in Fig. 4). It can be visualized a certain degree of scatter, in particular for the spheres, most likely due to the different experimental set-ups and procedures for data reduction employed in each of the literature sources.

Eq. (14) can be safely used under the following conditions (water and air as fluids):

$1.5 \le d_{eq}$ [mm] ≤ 6;	$15.4 \le a \le 54$;	$2.4 \le Re_L \le 200$
$0.00059 \le u_L$ [m/s] ≤ 0.024;	$0.31 \le \phi \le 1$;	$0.028 \le Re_G \le 300$
$0.00012 \le u_G$ [m/s] ≤ 1.06		

Despite the fact that Eq. (14) was obtained using water and air, it is very likely that it can also be suitable for fluids with similar Pr numbers, particularly for the liquid phase.

It should be pointed out that Eq. (14) has different ranges of applicability than those for Nu_w (Eq. (10)), due to different sources of experimental data used in each regression.

It is interesting to test the performance of the correlation (Eq. (14)) when the main geometric and operating variables are modified.

Fig. 5 presents the variation of k_{er} in terms of L for three sizes of spheres and similar values of the gas flow rate. Experimental data for the lowest particles diameter ($d_p = 1.5$ mm and 3 mm, $a = 34.3$ and 17.1, respectively) were obtained by Mariani et al. [11], while the data for spheres with the highest diameter (4.3 mm, $a = 17.7$) were reported by Matsuura et al. [28]. It is clear from Fig. 5 that k_{er} always increases as d_p increases irrespective of the value of the bed to particle diameter ratio. Eq. (14) is able to tightly capture the described behavior.

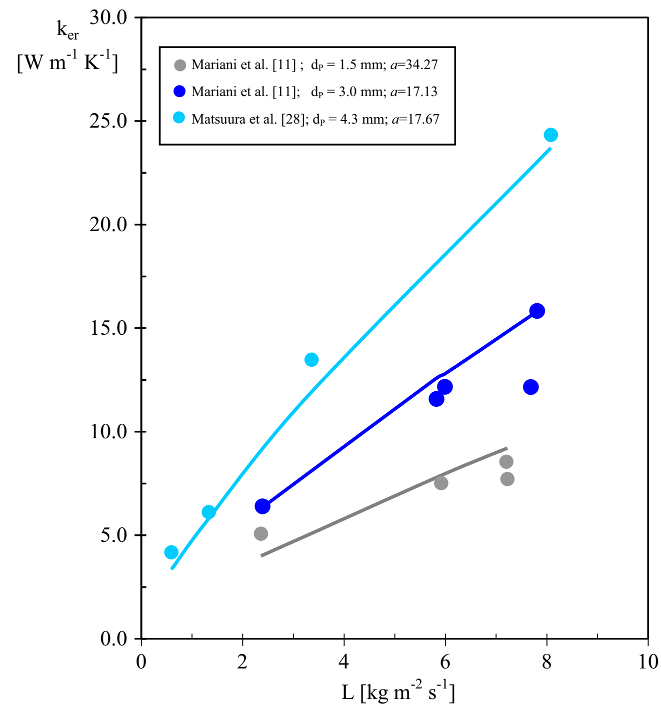

Fig. 5. Effect of d_p on k_{er} for spheres. Symbols: experimental data. Continuous lines: predictions from Eq. (14).

Fig. 6 presents k_{er} in terms of Re_L for the experimental data reported by Borremans et al. [26] and estimates from Eq. (14),

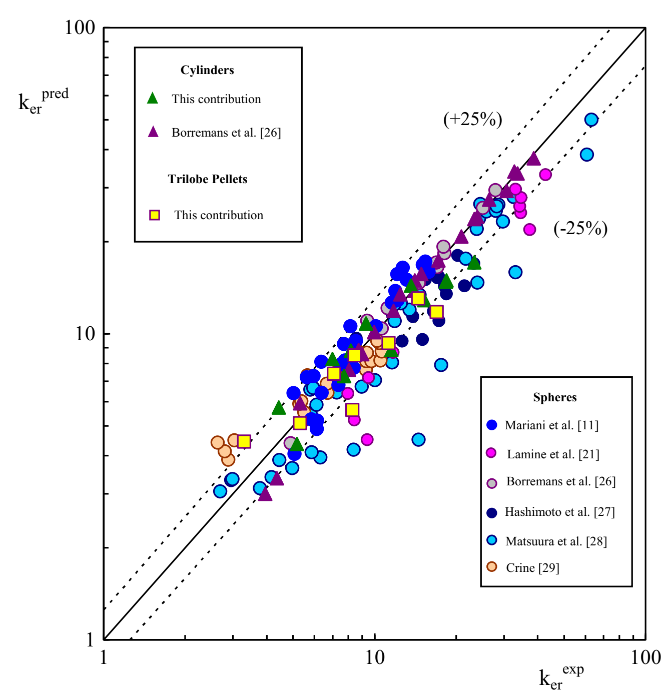

Fig. 4. Parity plot of experimental and predicted (Eq. (14)) values of k_{er}. (See above-mentioned references for further information.)

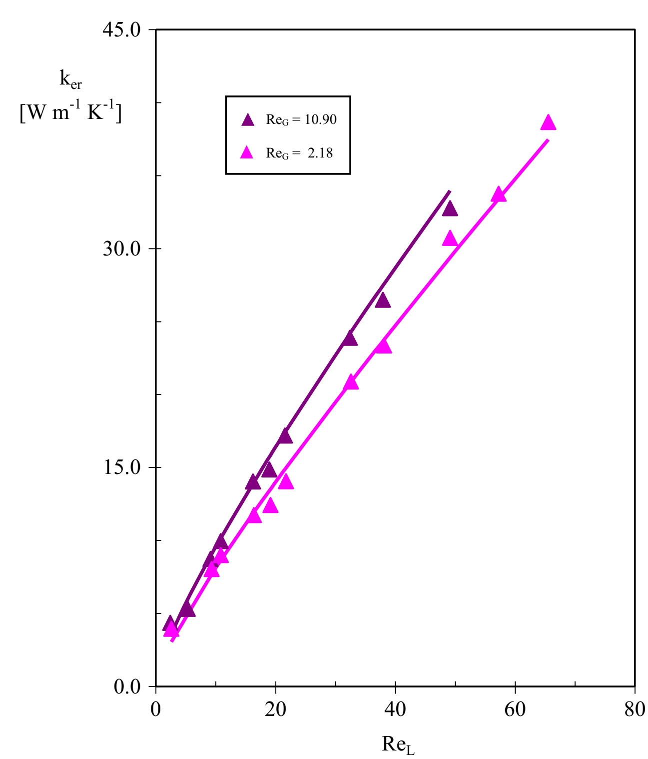

Fig. 6. k_{er} versus Re_L for cylinders. Symbols: Borremans et al. [26] experimental data ($d_{eq} = 1.85$ mm; $\phi = 0.43$; $a = 54$). Continuous lines: predictions from Eq. (14).

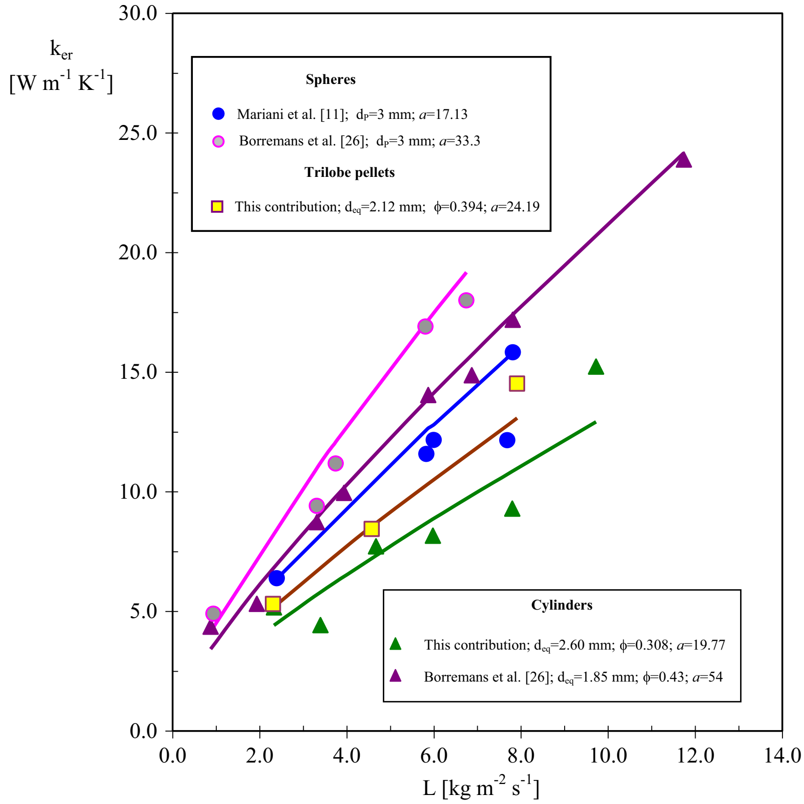

Fig. 7. k_{er} versus L for different particle shapes. Symbols: experimental data. Continuous lines: predictions from Eq. (14).

for cylindrical particles and two values of G. As happens for spheres, the greater L the greater k_{er}. In addition, k_{er} slightly increases as Re_G does (increasing Re_G five times leads to values of k_{er} around 20% higher). A remarkable agreement between experimental values and results from Eq. (14) can be appreciated.

Predictions from Eq. (14) and experimental values of k_{er} from different sources including cylinders and spheres are compared in Fig. 7. Two sets of data for 3 mm spheres are included (Borremans et al. [26] and Mariani et al. [11]). A satisfactory agreement is evident.

The effects of the particle shape and size and tube size were introduced in Eq. (14) by means of three geometrical magnitudes: the equivalent diameter d_{eq}, the particle aspect ratio ϕ, and the bed to particle diameter ratio a. Eq. (14) seems to appropriately combine the incidence of each magnitude. Nonetheless, it should be noted that a limited number of non-spherical particles have been involved in fitting the parameters of Eq. (14). Experimental data in the range $0.5 < \phi < 1$ would be desirable to further test Eq. (14).

4.3. Analysis of the overall bed to wall heat transfer resistances

It was discussed in Section 4.1 that values of Nu_w are significantly lower for cylindrical particles (circular cylinders and trilobes) than for spheres, at least for bed to particle diameter ratios a larger than 15. Then, it becomes important to disclose the effect of particle shape on the ratio between the wall thermal resistance ($R_w = 1/h_w$) and the overall thermal resistance of the bed ($R_T = 1/h_T$). This feature will be analyzed in this section when the gas and liquid streams solely exchange heat with the wall (*i.e.*, in the absence of catalytic reactions), as was the case of the experimental conditions considered in this contribution. Assuming for simplicity a uniform wall temperature and axial positions far enough from the inlet (*i.e.*, negligible *entry effects*) that only the term corresponding to the smallest eigenvalue b_1 in Eq. (6a) is significant,

$$\frac{T_w - T}{T_w - T_0(0)} = \frac{4C_1 \exp\left(-b_1^2 z^*\right)}{b_1^2\left[1 + (b_1/Bi)^2\right]} \tag{15}$$

where $Bi = (h_w R_t)/k_{er}$ and b_1 is the smallest root of $Bi\, J_0(b_1) = b_1 J_1(b_1)$.

The overall heat transfer coefficient h_T between the bed and the wall is defined as,

$$q = h_T(T_w - \bar{T}) \tag{16}$$

where $\bar{T}$ is the radially averaged temperature value.

An overall heat conservation equation can be written on a differential length dz as:

$$q\ (2\pi R_t dz) = \pi R_t^2 \left(LC_{pL} + GC_{pG}^*\right) d\bar{T} \tag{17}$$

Then, combining (16) and (17)

$$h_T = \frac{R_t}{2} \frac{\left(LC_{pL} + GC_{pG}^*\right)}{(T_w - \bar{T})} \frac{d\bar{T}}{dz} \tag{18}$$

If (15) is used to evaluate $\bar{T}$ and $d\bar{T}/dz$, the following expression results for h_T

$$h_T = k_{er} \frac{b_1^2}{2R_t} \tag{19}$$

The detailed procedure to link h_T with k_{er} and h_w can be found in Barreto and Martínez [30].

To avoid the evaluation of b_1, the following approximate expression proposed by Bruno et al. [31], which presents a maximum error of 0.9%, is employed:

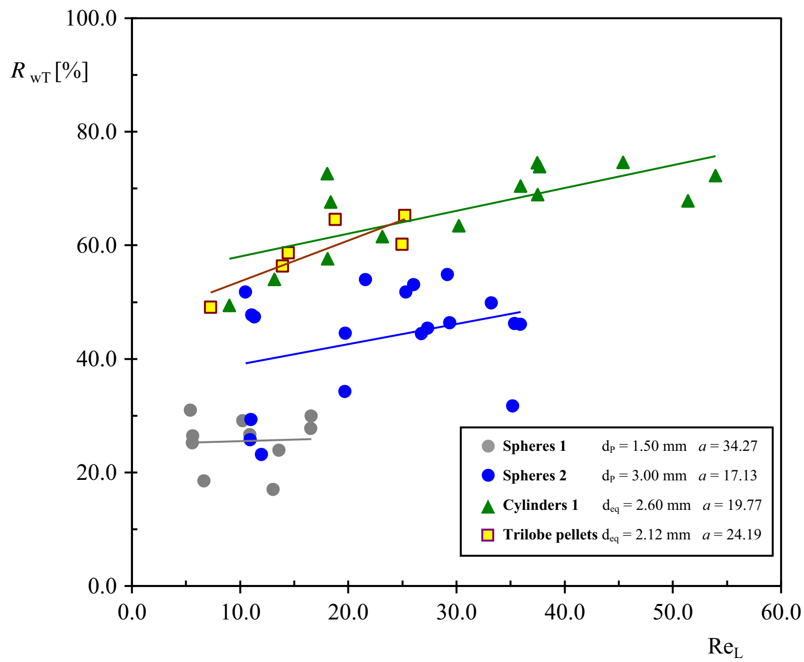

Fig. 8. Relative wall to bed heat transfer resistances ($R_{wT} = h_T/h_w$) versus Re_L.

$$h_T = \frac{h_w}{\sqrt{1 + 0.5Bi + 0.12(Bi)^2}} \quad (20)$$

Fig. 8 shows the relative heat transfer resistance at the bed wall, defined as $R_{wT} = h_T/h_w$, versus Re_L, calculated with the experimental values of h_w and k_{er} for the set of particles in Table 1, but excluding cylinders 2. Continuous curves are trend-lines, just included for visualization purposes. It is evident from Fig. 8 that the non-spherical particles (cylinders 1 and trilobe pellets) present higher relative resistance at the bed wall than spheres, in particular, when the comparison is performed between particles of similar bed to particle diameter ratio a (spheres 2 versus cylinders 1 and trilobe pellets), thus stressing an important effect of the particle shape. On the other hand, it should emphasized that, in spite of relatively large values of a for cylinders and trilobe pellets, the level of wall thermal resistances is most significant.

5. Conclusions

The two-dimensional pseudo-homogeneous plug flow model (2DPPFM) with two thermal parameters (effective radial thermal conductivity, k_{er} and wall heat transfer coefficient, h_w) has been employed to analyze new experimental heat transfer data for circular cylinders of two sizes and for trilobe particles along with literature information. In line with the conclusion previously discussed by Mariani et al. [18] for spherical packings, it is verified in this contribution that the 2DPPFM cannot suitably account for the thermal behavior of large cylinders leading to low ratios between bed diameter and equivalent particle diameter (a). Further analysis described in this work was therefore restricted to experimental data involving $a > 15$.

Correlations to predict h_w and k_{er} for particles of different sizes and shapes and a wide range of liquid (L) and gas (G) superficial mass velocities have been proposed. The correlation for h_w (Eq. (10)) was based on experimental data for spheres from Mariani et al. [11] and those presented here for circular cylinders and trilobes. The effect of G was found to be very weak while the effect of L is strong and accounted for by the correlation nearly in the form $h_w \propto L^{0.7}$. The effect of the particle shape on h_w could be appropriately described in terms of the diameter to length ratio ϕ (aspect ratio) of the particles. The average relative deviation between experimental and predicted values of h_w was 15.2%.

Aiming to elaborate a correlation to estimate k_{er} (Eq. (14)) the data introduced here and those from several literature sources were employed. Concerning the contribution of the liquid phase convection, the form of Eq. (14) turned out to be similar to those employed to predict the k_{er} in single phase-flow in packed beds, when compared on the basis of the liquid interstitial velocity. In this way, the liquid saturation β_T is explicitly introduced in Eq. (14). The effect of G arises indirectly through its effect on β_T. The influence of the size and shape of particles on k_{er} was properly accounted for by employing the equivalent diameter d_{eq} and the aspect ratio ϕ. The proposed correlation for k_{er} represents satisfactorily an extensive set of experimental data from different sources involving a wide range of operating and geometric conditions, different experimental set-ups and procedures for data reduction. The average relative deviation between experimental and predicted k_{er} for the whole set of data was 15.7%.

Acknowledgements

The authors wish to thank the financial support of the following Argentine institutions: ANPCyT-MINCyT (PICT'15 - 3456), CONICET (PIP # 0018) and UNLP (PID 2017–2020). N.J.M., O.M.M. and G.F.B. are Research Members of CONICET. M.J.T. holds a fellowship from CONICET.

References

[1] Ranade VV, Chaudhari RV, Gunjal PR. Trickle bed reactors – reactor engineering and applications. Oxford: Elsevier; 2011.
[2] Krishna R, Sie ST. Strategies for multiphase reactor selection. Chem Eng Sci 1994;49:4029–65.
[3] Zhu X. A study of radial heat transfer in fixed bed Fischer-Tropsch synthesis reactors [Ph.D. dissertation]. 2013: University of the Witwatersrand; 2013.
[4] Zhu X, Lu X, Liu X, Hildebrandt D, Glasser D. Heat transfer study with and without Fischer-Tropsch reaction in a fixed bed reactor with TiO_2, SiO_2, and SiC supported cobalt catalysts. Chem Eng J 2014;247:75–84.

[5] Mederos FS, Ancheyta J, Chen J. Review on criteria to ensure ideal behaviors in trickle-bed reactors. Appl Catal A 2009;355:1–19.
[6] Strasser W. CFD study of an evaporative trickle bed reactor: mal-distribution and thermal runaway induced by feed disturbances. Chem Eng J 2010;161:257–68.
[7] Germain AH, Lefebvre AG, L'homme GA. Experimental study of a catalytic trickle bed reactor. Adv Chem 1974;133:164–80.
[8] Taulamet MJ, Mariani NJ, Barreto GF, Martínez OM. A critical review on heat transfer in trickle bed reactors. Rev Chem Eng 2015;31:97–118.
[9] Brunner KM, Perez HD, Peguin R, Duncan JC, Harrison LD, Bartholomew CH, et al. Effects of particle size and shape on the performance of a trickle fixed-bed recycle reactor for Fischer-Tropsch synthesis. Ind Eng Chem Res 2015;54:2902–9.
[10] Heidari A, Hashemabadi SH. CFD study of diesel oil hydrotreating process in the non-isothermal trickle bed reactor. Chem Eng Res Des 2015;94:549–64.
[11] Mariani NJ, Martínez OM, Barreto GF. Evaluation of heat transfer parameters in packed beds with cocurrent downflow of liquid and gas. Chem Eng Sci 2001;56:5995–6001.
[12] Wang D, Fan L-S. Particle characterization and behavior relevant to fluidized bed combustion and gasification systems. In: Scala F, editor. Fluidized bed technologies for near-zero emission combustion and gasification. Elsevier; 2013. p. 42–76.
[13] Larachi F, Illiuta I, Chen M, Grandjean BPA. Onset of pulsing in trickle beds: evaluation of current tools and state-of-the-art correlation. Can J Chem Eng 1999;77:751–8.
[14] Charpentier JC, Favier M. Some liquid holdup experimental data in trickle-bed reactors for foaming and nonfoaming hydrocarbons. AIChE J 1975;21:1213–8.
[15] Tosun G. A study of concurrent downflow of nonfoaming system in packed beds. 1. Flow regime: search for a generalized flow map. Ind Eng Chem Process Des Dev 1984;23:29–35.
[16] Mariani NJ. Transferencia de calor en sistemas multifásicos [Tesis Doctoral]. Universidad Nacional de La Plata; 2000.
[17] Taulamet MJ. Fenómenos de transporte y reacción química en lechos fijos. Influencia de la forma del relleno catalítico [Tesis Doctoral]. Universidad Nacional de La Plata; 2015.
[18] Mariani NJ, Mazza GD, Martínez OM, Cukierman AL, Barreto GF. On the influence of liquid distribution on heat transfer parameters in trickle bed systems. Can J Chem Eng 2003;81:814–20.
[19] Taulamet MJ, Mariani NJ, Barreto GF, Martínez OM. Estimation of overall heat transfer coefficients in packed beds with cocurrent downflow of gas and liquid. Fuel 2014;138:176–82.
[20] Giese M, Rottschafer K, Vortmeyer D. Measured and modeled superficial flow profiles in packed beds with liquid flow. AIChE J 1998;44:484–90.
[21] Lamine AS, Gerth L, Le Gall H, Wild G. Heat transfer in a packed bed reactor with cocurrent downflow of a gas and a liquid. Chem Eng Sci 1996;51:3813–27.
[22] Ranz WE. Friction and transfer coefficients for single particles and packed beds. Chem Eng Prog 1952;48:247–53.
[23] Larachi F, Laurent A, Midoux N, Wild G. Experimental study of a trickle-bed reactor operating at high pressure: two-phase pressure drop and liquid saturation. Chem Eng Sci 1991;46:1233–46.
[24] Fahien RW, Smith JM. Mass transfer in packed beds. AIChE J 1955;1:28–37.
[25] Dixon AG. Fixed bed catalytic reactor modeling – the radial heat transfer problem. Can J Chem Eng 2012;90:505–27.
[26] Borremans D, Rode S, Carré P, Wild G. The influence of the periodic operation on the effective radial thermal conductivity in trickle bed reactors. Can J Chem Eng 2003;81:795–801.
[27] Hashimoto K, Murayoma K, Nagata S, Fujiyoshi K. Effective radial thermal conductivity in concurrent flow of gas and liquid through packed bed. Int Chem Eng 1976;16:720–7.
[28] Matsuura A, Hitaka Y, Akehata T, Shirai T. Effective radial thermal conductivity in packed beds with gas-liquid downflow. Kagaku Kogaku Rombunshu 1979;5:269–74.
[29] Crine M. Heat transfer phenomena in trickle-bed reactors. Chem Eng Commun 1982;19:99–114.
[30] Barreto GF, Martínez OM. Prediction of overall heat transfer coefficients for the simulation of multitubular catalytic fixed bed reactors. Trends Heat Mass Moment Transf 1992;2:1–33.
[31] Bruno SP, Barreto GF, González MG. Effect of the geometric characteristics of commercial catalysts for steam reforming. Chem Eng J 1988;39:147–56.